A source model for earthquakes near the nucleation dimension

Camilla Cattania[1]

[1]Department of Earth, Atmospheric, and Planetary Sciences, Massachusetts Institute of Technology, Cambridge, MA

Abstract

[1] Earthquake self-similarity is a controversial topic, both from an observational and theoretical standpoint. Theory predicts the existence of a finite nucleation dimension, implying a break of self-similarity below a certain magnitude. While observations of non self-similar earthquake behavior have been reported, their interpretation remains debated, since estimating source properties is challenging due to trade-offs between source and path effects and assumptions on the underlying source model, which often assume self-similarity in the first place.

Here I introduce a source model that accounts for earthquake nucleation, and quantify how the nucleation phase affects ground motion. The model consists of an equation of motion for a circular rupture front (derived from fracture mechanics) and far-field displacement pulses and spectra. The onset of ground motion is characterized by exponential growth with characteristic timescale $t_0 = R_0/v_r$, with R_0 the nucleation dimension and v_r a limit rupture velocity. As a consequence, normalized displacements have a constant source duration, proportional to the nucleation length rather than the source dimension. For ray paths normal to the fault, the exponential growth results in a Boatwright spectrum with $n = 1$, $\gamma = 2$ and corner frequency $f_c = 1/t_0$. For other orientations, the spectrum has an additional sinc$(\cdot)$ term with a corner frequency related to the travel time delay across the asperity. Seismic moments scale as $M_0 \sim R(R - R_0)R_0$, where R is the size of asperity, becoming vanishingly small as $R \to R_0$. Consequently, stress drops estimated from M_0 and f_c are smaller than the nominal stress drop, and they decrease with decreasing magnitude, consistent with several seismological studies. The constant earthquake duration is also in agreement with reported microseismicity, providing an estimate of the nucleation length:

[1]The authors acknowledge there are no conflicts of interest recorded.

for $0 < M_W < 2$ events studied by Lin et al. (2016) in Taiwan, a model with a nucleation length between $45 - 80$m provides a good fit to observed durations.

1 Introduction

The concept of earthquake self-similarity (Aki, 1967) is often assumed in seismology, and it is supported by a large body of observations indicating that the stress drop remains constant over a wide range of magnitudes (e.g. Abercrombie, 1995, 2021, and references therein). In contrast, observations suggesting a break in self-similarity have been reported in local studies (e.g. Harrington & Brodsky, 2009; Bouchon et al., 2011; Lin et al., 2016; Imanishi & Uchide, 2017; Trugman & Shearer, 2017; H. Wang, Ren, Wen, & Xu, 2019; Mayeda, Malagnini, & Walter, 2007; Bindi, Spallarossa, Picozzi, & Morasca, 2020), even though their interpretation is hampered by well known artifacts due to trade-offs between path and source effects and attenuation of high-frequencies (Abercrombie, 1995; Ide, Beroza, Prejean, & Ellsworth, 2003; Abercrombie, 2021).

Scale invariance typically arises from physical processes without a characteristic length scale. In contrast, commonly used friction laws contain a characteristic slip distance that determines the weakening behavior. This results in characteristic lengths: Ruina (1983) first postulated the existence of a finite nucleation length from a linear stability analysis, later confirmed in numerical studies of faults with rate-state friction (Dieterich & Linker, 1992; Rubin & Ampuero, 2005), and observed experimentally (Leeman, Saffer, Scuderi, & Marone, 2016; McLaskey, 2019).

Self-similarity is often inferred from the scaling between seismic moment and corner frequency. The seismic moment produced by a circular rupture of radius R and stress drop $\Delta\tau$ is given by (Eshelby, 1957):

$$M_0 = \frac{16}{7}\Delta\tau R^3. \tag{1}$$

Assuming that the earthquake duration T scales linearly with its radius, and taking the corner frequency $f_c \approx 1/T$ leads to the predicted the scaling: $M_0 \sim f_c^{-3}$. A large source of uncertainty is the constant of proportionality between corner frequency and source dimension, which strongly depends on the chosen source model. Self-similar models, such as those proposed by Madariaga (1976) and Sato and Hirasawa (1973), assume that ruptures start at the center of a circular asperity and propagate at constant velocity. Recent studies have relaxed some of these assumptions, by considering the effect of a cohesive zone (Kaneko & Shearer, 2014), elliptical and unilateral rupture propagation (Kaneko & Shearer, 2015), irregular ruptures on heterogeneous faults (Lin & Lapusta, 2018) and earthquakes propagating as pulses rather than cracks (Y. Wang & Day, 2017). These factors introduce variability in estimating the source dimension, which can strongly affect stress drop estimates due to the cubic dependence on R in eq. 1. To the best of my knowledge, none of the proposed source models explicitly accounts for the increase in slip and rupture velocity during the nucleation phase. A better characterization of the seismic signature of earthquake nucleation would facilitate the interpretation of observed breaks in self-similarity, and help bridge the gap between laboratory studies and actual faults by estimating the nucleation dimension on natural faults.

To this end, here I use fracture mechanics to derive a kinematic source model that accounts for earthquake nucleation, and describe its predictions on seismological observables such as far-field pulse duration and stress drop estimates. I show that the spectrum is characterized by two corner frequencies and an apparent constant source duration for small earthquakes, as confirmed by fully dynamic rupture simulations. In section 3 I discuss these findings in the context of seismological studies, and show that the existence of a finite nucleation dimension can explain observations of constant source duration (Lin et al., 2016; Harrington & Brodsky, 2009; Lengliné, Lamourette, Vivin, Cuenot, & Schmittbuhl, 2014) with a nucleation dimension of the order of $45 - 80$m. The model also predicts an increase in stress drop with magnitude, as inferred in several studies (Mayeda et al., 2007; Bindi et al., 2020; Trugman & Shearer, 2017, among others). Other model predictions, such as the double corner frequency and its dependence on observation angle, may be used to further test this hypothesis and provide estimates of the nucleation dimension in the future.

2 Theoretical source model

The classical scaling between rupture dimension and duration follows from the assumption of constant rupture velocity, which breaks down during nucleation when the rupture front accelerates. To estimate earthquake duration in this regime we need an equation of motion for the rupture front, which can be derived from fracture mechanics. Following Freund (1990), the motion of the rupture front is controlled by a balance between fracture energy and the mechanical energy provided by slip with the crack:

$$G(r, \dot{r}) = \Gamma, \tag{2}$$

where Γ is the fracture energy and G the dynamic energy release rate, which quantifies the stress concentration ahead of the rupture and is a function of the its dimension r and propagation velocity $\dot{r}$. G is related to the dynamic stress intensity factor K by

$$G = A(\dot{r})\frac{K(r,\dot{r})^2}{2\mu'}, \tag{3}$$

where A is a universal function of crack speed (different for each mode of deformation) and μ' is the shear modulus μ for antiplane deformation and $\mu/(1-\nu)$, with ν the Poisson's ratio, for plane strain deformation. The dynamic stress intensity factor is related to the static stress intensity factor $K(r,0)$ as follows:

$$K(r,\dot{r}) = k(\dot{r})K(r,0), \tag{4}$$

where $k(\dot{r})$ a universal function of rupture velocity. To simplify notation, I write the static stress intensity factor as $K(r)$. The equation of motion of the crack tip is then given by

$$K(r) = \left(\frac{2\mu'\Gamma}{A(\dot{r})k(\dot{r})^2}\right)^{1/2}. \tag{5}$$

The product $A(\dot{r})k^2(\dot{r})$ can be approximated as $1-\dot{r}/v_f$, where v_f is the terminal rupture velocity (shear wave velocity for mode III cracks and the Rayleigh wave velocity for mode II cracks, Freund (1990)). For simplicity, in what follows I neglect the difference between mode II and mode III, and assume that the crack is circular; the same results, within a factor of order one, are expected to apply for the elliptical crack in the case of mixed-mode propagation.

I assume the initial crack radius satisfies eq. 5 for $\dot{r} = 0$. For a constant fracture energy, eq. 5 can then be written as

$$K(r) = \frac{K(R_0)}{\sqrt{1-\dot{r}/v_f}}. \tag{6}$$

The stress intensity factor for a circular crack of radius r is $K(r) \propto \Delta\tau\sqrt{r}$; for a constant stress drop, combining this with eq. 6 yields the following expression for crack tip velocity as a function of radius:

$$v_r = \dot{r} = v_f\left(1 - \frac{R_0}{r}\right). \tag{7}$$

Since $\dot{r}(R_0) = 0$, solving for crack position as a function of time with initial condition $r(0) = R_0$ gives $r(t) = R_0$ at all times. Instead, I assume that the crack exceeds the nucleation dimension by a small amount: $r/R_0 = 1+\epsilon$, with $\epsilon \ll 1$. The crack radius then grows as

$$r/R_0 = 1 + W\left(ge^{t/t_0}\right) \tag{8}$$

$$v_r/v_f = 1 - \left[1 + W\left(ge^{t/t_0}\right)\right]^{-1} \tag{9}$$

where $W(\cdot)$ is the Lambert omega function, $t_0 = R_0/v_f$ is a characteristic timescale, and $g = W^{-1}(\epsilon) \approx \epsilon$.

2.1 Far-field pulses and amplitude spectra

The kinematic source model presented above is the starting point to find far-field ground motion and source spectra for an accelerating crack. Far-field pulses and spectra are obtained from body wave displacements for a point source shear dislocation (Aki & Richards, 1980):

$$\mathbf{u}(\mathbf{x},t) = \frac{\mathbf{A}^{p,s}}{4\pi\rho c_{p,s}^3 D}\dot{M}_0\left(t\right), \tag{10}$$

where ρ is the density, $c_{p,s}$ is the wave velocity for P or S waves, $\mathbf{A}^{p,s}$ are their respective radiation patterns, D is the distance between source and receiver, and $\dot{M}_0$ the moment rate given by

$$\dot{M}_0(t) = \mu \int\int_s v(t - d/c_{p,s})\ ds, \tag{11}$$

with μ the shear modulus, v the slip velocity, and d the distance between the receiver and individual points on the fault surface. A constant stress drop crack propagating at speed v_r has the following velocity profile:

$$v(\rho) = \frac{24\Delta\tau}{7\pi\mu}\frac{r(t)}{\sqrt{r(t)^2-\rho^2}}v_r(t), \tag{12}$$

where $\Delta\tau$ is the stress drop, $r(t)$ the crack radius, and ρ radial distance within the crack (Sato & Hirasawa, 1973). I use eq. 9 for $v_r(t)$ and calculate far-field ground motion by numerically integrating eq. 11 for a range of observation angles θ. Examples of far-field displacement pulses can be seen in Fig. 1. After reaching the edge of a circular asperity, the rupture decelerates and arrests: in Appendix A I derive an equation of motion from energy arguments analogous to those in the previous section, assuming a region of negative stress drop $\Delta\tau_{out}$ surrounding the asperity, due for example to velocity-strengthening friction. The strength of the barrier is quantified by the parameters $\alpha = \Delta\tau_{out}/\Delta\tau - 1$. I find that rupture arrest has a minor effect on source properties (Fig. 1), and in the rest of the paper I focus on the case $\alpha = -2$, which corresponds to a stress barrier equal and opposite to the stress drop.

2.1.1 Pulses and spectra for $\theta = 0$

Fig. 2(a,b) shows the normalized far-field spectra for the Sato and Hirasawa (1973) model with constant rupture velocity and the accelerating rupture model. As expected, the classic model assuming constant rupture velocity produces pulses of increasing duration with increasing earthquake dimension R. In contrast, the accelerating model produces longer pulses due to the slower average rupture velocity, and with approximately constant duration. This is one of the main results of this study and will be discussed in more detail below. The theoretical model presented above is a simplified representation of the more complex elasto-frictional processes

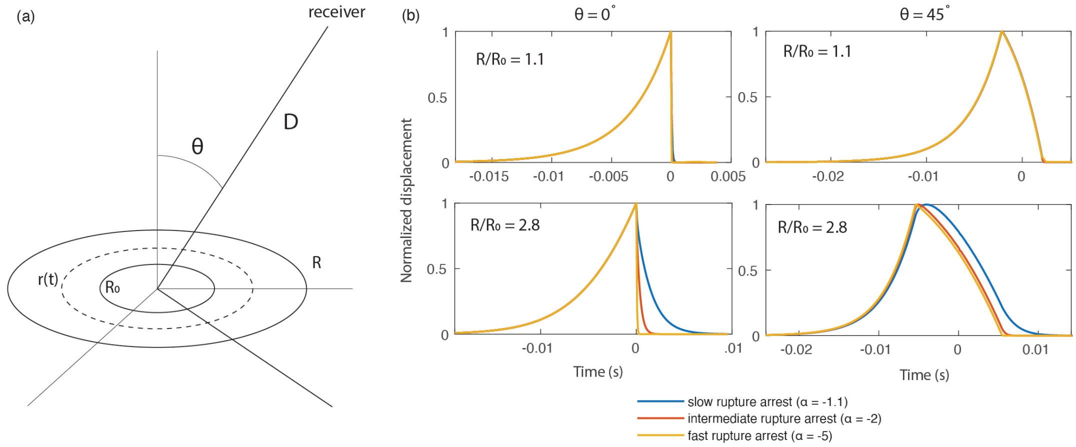

Figure 1: (a) coordinate system and sketch of rupture propagation starting at the nucleation radius R_0 and propagating up to asperity radius R with variable rupture velocity. (b) examples of normalized far-field S-wave pulses for two values of R/R_0 and θ, with $c_s = 3600\text{m/s}$, $R_0 = 10\text{m}$. The deceleration seen for $\theta = 0$ is due to rupture arrest (see Appendix A).

taking place during nucleation and rupture propagation, and it contains several assumptions such as constant stress drop and rupture shape. Therefore, I also run fully dynamic rupture simulations of earthquake cycles on faults controlled by rate-state friction with the ageing law, using the numerical code of Lapusta and Liu (2009), described in Appendix C. Fig. 2c shows that normalized ground motion for events with $R_0 < R < 1.6R_0$ collapse on the same line and have approximately constant duration as predicted by the analytical model. As previously observed by Chen and Lapusta (2009) and Cattania and Segall (2019), asperities exceeding $R = approx R_0$ tend to produce lateral ruptures, not described by the circular model adopted here.

The constant duration can be understood from the equation of motion. For the observation angle $\theta = 0$ and in the far field, the time delay in eq. 10 is a constant, so the observed displacement is simply proportional to the integrated slip velocity. It can be shown that the integral is proportional to the product of crack area and rupture velocity:

$$u \sim r(t)^2 V_r(t), \tag{13}$$

where I omitted the constant time delay d/c in eq. 10 for convenience. For constant rupture velocity, far field displacements simply grow as rupture area or t^2, and if we define rupture duration as the time during which the normalized slip speed exceeds a certain value, the duration scales as $T \sim R/v_r$, as expected.

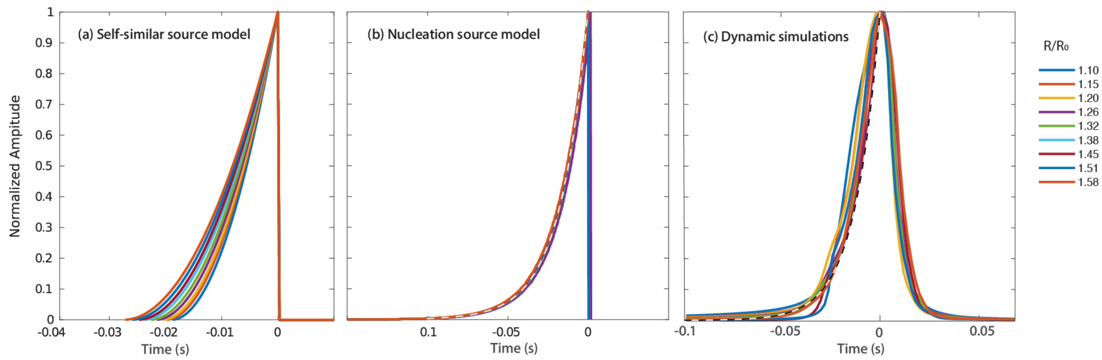

Figure 2: Normalized far-field displacements observed at $\theta = 0$. (a) Sato and Hirasawa (1973) model with constant rupture velocity. (b) kinematic modified model accounting for accelerating rupture, with instantaneous rupture arrest. (c) fully dynamic earthquake simulations. Dotted lines are theoretical expressions for $R \approx R_0$ ($u/u_f = \exp(-\Delta t/t_0)$). The nucleation length in panel (c) is estimated using the result from Rubin and Ampuero (2005) modified for a 3D crack (Cattania & Segall, 2019), and rupture velocity v_r equal to the shear wave speed, corresponding to the mode III edge of the rupture.

For the accelerating crack, both r and v_r are time-dependent. Early on, $v_r \approx 0$ and we can assume that the radius is approximately constant, so that far-field displacement is proportional to the rupture velocity given by eq. 9. In the early stages of nucleation, when $ge^{t/t_0} \ll 1$, the Lambert W-function can be approximated as $W(x) \approx x$ for $x \ll 1$ so that $\dot{r}/c \approx ge^{t/t_0}$. The normalized far-field displacement observed at a time t before the end of the rupture is then simply

$$\frac{u}{u_{max}} = \frac{v_r}{v_{r,\max}} = e^{-t/t_0}, \tag{14}$$

and it does *not* depend on the final radius but only on the time interval, so that all normalized curves collapse on the same line. This expression, shown by the dotted lines in Fig. 2(b,c), is in excellent agreement with the nucleation model and with the dynamic simulations. If we define the earthquake duration as the time when far-field displacements reach an arbitrary fraction of its peak value ($u = \phi u_f$), the event duration is given by

$$T = t_0 \log\left(\frac{1}{\phi}\right). \tag{15}$$

with $t_0 = \frac{R_0}{v_f}$. Finally, the Fourier transform of eq. 14 produces the following normalized amplitude spectrum:

$$|u(\omega)| = \frac{u_{max} t_0}{\sqrt{1 + \omega^2 t_0^2}}, \tag{16}$$

which corresponds to a Boatwright (1980) spectrum with $n = 1$, $\gamma = 2$, and corner frequency $\omega_c = 1/t_0$.

2.1.2 Pulses and source spectra for all observation angles

Displacement pulses and source spectra as a function of observation angle are derived in Appendix B; here I summarize the main results. The pulse duration is given by

$$T = t_0 \left[\log\left(\frac{1}{\phi}\right) + \log\left(\frac{e^{\Theta} - 2\phi \sinh\Theta}{e^{-\Theta}}\right) \right] \tag{17}$$

with $\Theta = R\sin\theta/ct_0$, c is the speed of P or S wave, R the asperity dimension, and ϕ the threshold defined in section 2.1.1. The first term in square brackets reflects the acceleration in slip velocity during nucleation, and it does not depend on R; the second term is associated with the time lag between radiation from opposite sides of the rupture, which increases with source radius and observation angle.

Finally, the spectrum of the moment rate function is given by

$$|\dot{M}_c(\omega)| = \frac{48\Delta\tau}{7}(R - R_0)R_0 R \ \mathrm{sinc}\left(\frac{\omega R \sin\theta}{c}\right)\frac{1}{\sqrt{\omega^2 t_0^2 + 1}}. \tag{18}$$

The spectrum has two corner frequencies, corresponding to the two characteristic timescales discussed above. The sinc$(\cdot)$ reflects the travel time difference between opposite ends of the rupture, while the Boatwright term, previously obtained for $\theta = 0$, reflects the exponential increase in rupture velocity (eq. 14), which is a function of nucleation length rather than asperity dimension.

Most seismological studies use a spectrum with a single corner frequency, which will fall between these values. This can be verified by fitting a Brune (1970) and a Boatwright (1980) models to the amplitude spectrum obtained from the nucleation source model (Fig. 3). Corner frequencies f_c and fall-off rates are estimated using a least-square fit weighted by the inverse of the frequency, in the frequency range $0.05 f_c < f < 10 f_c$ (Kaneko & Shearer, 2014). As expected, the Boatwright model correctly describes the spectrum for $\theta = 0$. For larger θ, the Brune model better captures the lower corner frequency (and hence source behavior), while Boatwright estimates are closer to the second corner frequency for small values of θ, up to about 20°.

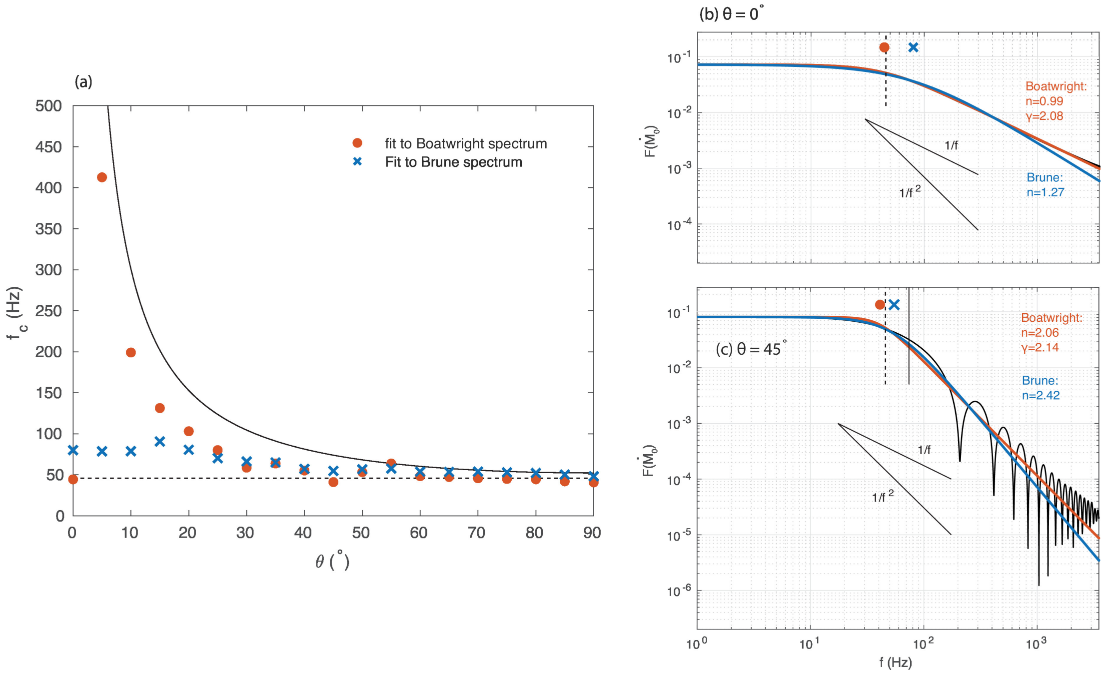

Figure 3: Corner frequency and fall-off exponents estimated by fitting a Brune and a Boatwright spectrum to the far-field displacements produced by an event near the nucleation dimension $R = 1.1R_0$ and fast rupture arrest ($\alpha = -5$). (a) Brune (cross) and Boatwright (circle) corner frequencies generally fall between the two theoretical corner frequencies predicted by eq. 18 associated with the rupture acceleration (dotted line) and to the delay between stopping phases (solid line). (b) Spectrum for $\theta = 0°$, close to the expected Boatwright spectrum for $R \approx R_0$, eq. 16. (c) Spectrum for $\theta = 45°$.

2.2 Seismic moment and stress drop scaling

The seismic moment is estimated from the zero-frequency asymptote of the moment rate function (Aki & Richards, 1980), and shown in Fig. 4(a). Moments are normalized by the moment that a constant stress drop crack of size R_0 would produce if it ruptured seismically: $M_{0,ref} = (16/7)\Delta\tau R_0^3$. While this value does not have an obvious physical interpretation, since eq. 1 does not apply in this limit, I introduce it for convenience, to facilitate interpretation of seismological observations in terms of a nucleation dimension. For sufficiently large asperities ($R \approx 2R_0$ or larger), seismic moments scale follow the classical scaling ($M_0 \sim R^3$, eq. 1); in contrast, the seismic moment for events near the nucleation dimension is lower than the classical result, since slip is released aseismically during the nucleation phase. In this case, seismic moments are given by eq. 18 for $\omega = 0$:

$$M_0 = \frac{48}{7}\Delta\tau R_0 R(R - R_0). \quad (19)$$

Note that the existence of a finite nucleation length does not translate to a lower bound in seismic moment: eq. 19 predicts arbitrarily small M_0, due to a small amount of seismic slip over a finite source.

If corner frequencies are inversely proportional to source dimension, stress drops can be estimated by plotting M_0 vs. f_c, and the term "stress drop" is often used to describe the scaling between these two quantities, even though some authors have argued against this use of the term (Atkinson & Beresnev, 1997). For small sources, the assumption that $f_c \sim R^{-1}$ clearly does not apply, as confirmed by the constant source duration for small θ (section 2.1.1). For easier comparison with observational studies, I define the measured stress drop as

$$\Delta\tau_m = \frac{7}{16}\frac{M_0 f_c^3}{k^3 c^3}, \quad (20)$$

where k is a constant of proportionality defined by the relationship $f_c = kc_s/R$. The value of k depends on assumptions about the source model; here I use $k = 0.21$, the value obtained by Madariaga (1976) for S-waves from dynamic simulations with constant rupture velocity $v_r = 0.9\beta$. I define corner frequencies as $f_c = 1/T$, where T is the duration defined as in eq. 15 with $\phi = 0.5$. Fig. 4(b) shows the measured stress drop for $\theta = 0$: since the source duration tends to a constant for $R \to R_0$, while seismic moments become vanishingly small, estimated stress drops are lower for small magnitude events. This effect is visible for events with moment magnitudes up to about $M_{w0} + 2.5$, at which point $\Delta\tau_m$ is close to the nominal stress drop.

3 Discussion

A finite nucleation dimension implies a break in self-similarity, and the traditional scaling relations between seismic moment and earthquake duration (or equivalently, stress drop) are not expected to hold for source dimensions close to the nucleation length. A departure from self-similarity, if observed, could therefore provide an indirect in-situ estimate of the nucleation dimension, and a comparison to laboratory or numerical experiments under which earthquake nucleation has been hypothesized and observed (Dieterich, 1992; McLaskey, 2019). Here I presented a simple analytical source model for events near the nucleation dimension, and outline seismological observations and scaling relations that might reveal a break in self-similarity. Like all source models assuming a circular rupture propagating on a uniform fault, this model doesn't

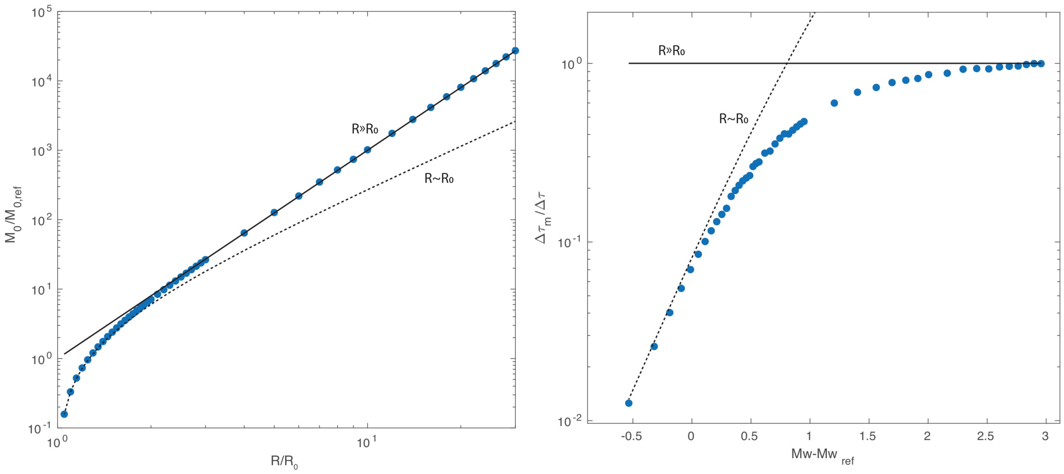

Figure 4: Left: normalized seismic moment vs. normalized radius predicted by the theoretical source model (section 2). The solid and dotted lines indicate analytical results for $R \gg R_0$ (eq. 1) and $R \approx R_0$ (eq. 19).

capture the complexity of real earthquakes, which can have complex source time functions even at small magnitude (Abercrombie, 2021) and increased variability in stress drop due to rupture geometry and other factors (Kaneko & Shearer, 2014, 2015; Lin & Lapusta, 2018; Y. Wang & Day, 2017). But while the model will not capture all details of real earthquakes, the existence of a finite nucleation dimension fundamentally modifies source properties and scaling relations, and these first-order features likely persist in more realistic cases.

3.1 Observations of constant earthquake duration

The first result of this study is that earthquakes near the nucleation dimension appear to constant duration, given by eq. 17. This perhaps surprising result arises from the early exponential acceleration in rupture velocity, and from the definition of "duration" as the time during which the far-field pulse exceeds a fraction of the final value. Constant earthquake duration across a range of magnitudes has indeed been reported for small events by several authors: Harrington and Brodsky (2009) for microearthquakes along the San Andreas and secondary faults, Lin et al. (2016) for repeaters along the Chengdu fault in Taiwan and Lengliné et al. (2014) for fluid induced earthquakes. Lin et al. (2016) estimated earthquake durations from source time functions, and are defined them as twice the time during which the moment rate exceeds 50% of the peak value. These observations can be directly compared to the prediction from eq. 17 and seismic moments from eq. 19, as shown in Fig. 5. The nucleation model provides a better fit that the classical scaling, and can explain the observed source duration with a nucleation

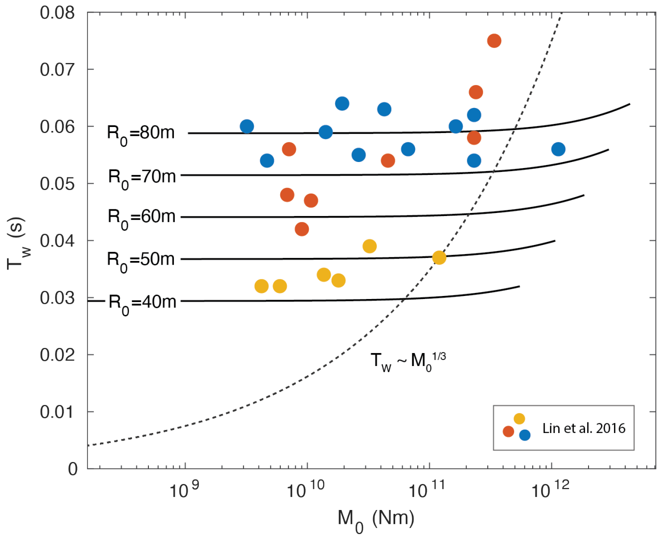

Figure 5: Seismic moments and source durations from Lin et al. (2016), with each color corresponding to a different cluster. Black lines indicate the predicted scaling for sources near the nucleation dimension (eq. 17, 19) with $\theta = 28°$, $v_r = 2505$m/s, $c = 5700$m/s, $\phi = 1/2$ (from Lin et al. (2016)), $\Delta\tau = 3$MPa and $\mu = 30$GPa. Note that durations here are twice the definition used in the text, for consistency with Lin et al. (2016). The dotted line indicates the classical $T \sim M_0^{1/3}$ scaling for a 3MPa stress drop.

dimension of the order of about $45 - 80$m. This is consistent with estimates for typical values of frictional parameters assuming rate-state friction (e.g. Rubin & Ampuero, 2005; Chen & Lapusta, 2009; Cattania & Segall, 2019).

3.2 Observations of magnitude dependent stress drops

Evidence for breaks in self-similarity in larger datasets remains a subject of intense debate (for a review, see Abercrombie (2021)). When estimates of corner frequencies and seismic moment are plotted together for several datasets, stress drops appear to be remarkably constant across a broad range of magnitude, including millimeter scale events recorded in laboratory (Selvadurai, 2019; Yoshimitsu, Kawakata, & Takahashi, 2014), centimeter scale earthquakes in deep mines (Kwiatek & Ben-Zion, 2013), up to kilometer scale earthquakes (e.g. Baltay, Ide, Prieto, and Beroza (2011); Zollo, Orefice, and Convertito (2014); Abercrombie (2021) and references therein). However, observed stress drops span several orders of magnitude, and individual studies have reported trends of increasing stress drops with magnitude in Italy (Bindi et al., 2020; H. Wang et al., 2019; Malagnini, Scognamiglio, Mercuri, Akinci, & Mayeda, 2008)

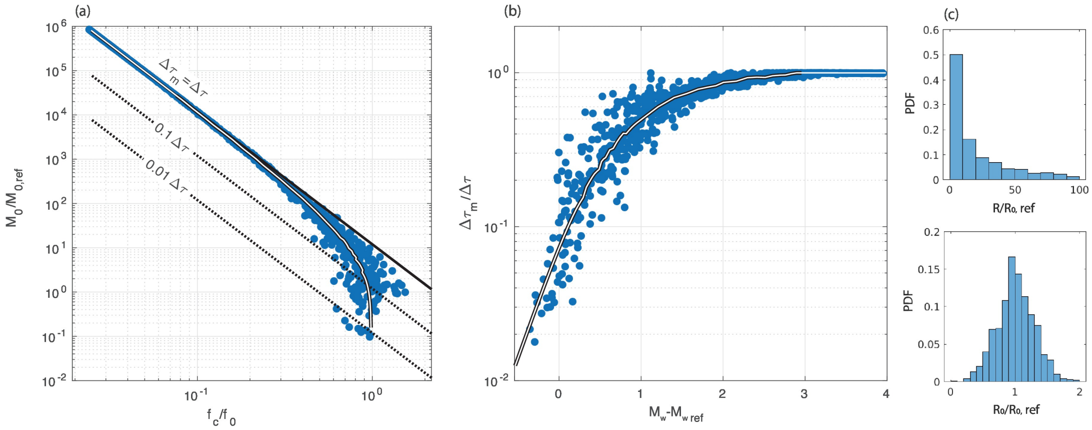

Figure 6: (a) Normalized seismic moment vs. normalized corner frequency, obtained from the scaling shown in Fig. 4 (lines) with variable nucleation lengths drawn from a Gaussian distribution. (b) Ratio between measured and true stress drop vs. magnitude relative to the reference magnitude. (c) PDF of normalized asperity dimensions (top) and nucleation lengths (bottom).

and California (Mayeda et al., 2007; Trugman & Shearer, 2017), among others; a consistent observation across many studies is the increased scatter in stress drop for small magnitude earthquakes. These observations are notoriously difficult due the trade-off between source and path effects, including frequency and depth dependent attenuation (e.g. Abercrombie, 1995; Shearer, Abercrombie, Trugman, & Wang, 2019), and hence it remains unclear whether the observed decrease in stress drop for small earthquakes is a source or a path effect.

With these caveats in mind, it is worth noting that theoretical source model presented here provides an explanation for the reported deviations from the $M_0 \sim f_c^{-3}$ scaling, as well as the increase in scatter for small magnitude events. Since a fraction of slip is released aseismically during the nucleation phase, asperities close to the nucleation dimension have smaller seismic moment than predicted by the classical scaling. This effect, combined with the constant duration for small events, reduces stress drops by a factor of about 100 over 2 earthquake magnitudes (Fig. 4). The shape of the curve differs from reported observations, in which the trend persists up to large magnitudes and takes the form: $M_0 \sim f_c^{-(3+\epsilon)}$ (Kanamori & Rivera, 2004). The model could be better reconciled with the data, and reproduce its scatter, by accounting for spatial heterogeneity in nucleation length. I test this idea with a simple synthetic test. I start with a set of 1000 source radii randomly sampled from a uniform distribution in log-space; and a random sample of nucleation dimensions drawn from a Gaussian distribution centered at the reference nucleation dimension R_0, with a standard deviation equal to $0.3R_0$. This produces pairs of source-dimension and nucleation dimensions. I discard pairs with a nucleation dimension exceeding the source radius, since they would be aseismic (Chen & Lapusta, 2009; Cattania & Segall, 2019). For the remaining pairs, I obtain duration and moment by interpolating Fig. 4, and rescaling the result by the characteristic duration and moment for each the nucleation length. Given the scatter in the resulting plots (Fig. 6), it seems plausible that the trend would be interpreted as $M_0 \sim f_c^{-(3+\epsilon)}$, especially if low magnitude events are below the completeness magnitude and hence missing from the catalog. The model also predicts more stress drop variability at low magnitudes, consistent with observations.

To determine whether a finite nucleation dimension causes the observed non-similar scalings, other model predictions could be tested against data. For events with $\theta = 0$, the constant source duration produces constant corner frequency, and the spectrum takes the form of a Boatwright spectrum (eq. 16). For all other observation angles, the Boatwright spectrum is multiplied by a $\mathrm{sinc}(\cdot)$ term corresponding to the delay between phases emitted simultaneously from opposite ends of the source. Should these patterns be discernible in the data, they would corroborate the hypothesis that the existence of a finite nucleation dimension is responsible for observed breaks in self-similarity.

4 Conclusion

I introduce an analytical source model which accounts for acceleration in slip and rupture velocity as well as the finite size of the nucleation region. In the early phases of nucleation, the model predicts that far field displacements grows exponentially with time, producing a constant source duration and corner frequency. This is consistent with some observations of both tectonic and induced microseismicity, and implies a nucleation dimension of the order of tens of meters. Furthermore, the seismic moment decreases as more slip is accrued aseismically, causing a decrease in estimated stress drop. With the improvement of seismic networks and detection algorithms, future studies may be able to further verify these findings and test additional model predictions, such as the double corner frequency and variations of spectral properties with observation angle.

A Appendix: Rupture arrest

The fracture mechanics criteria in section 2 can also be applied to rupture arrest. I assume that the region outside an asperity of radius R experiences a stress increase $\Delta\tau_{in}$ during dynamic rupture (due, for example, to velocity-strengthening friction), adding a negative term to the stress intensity factor (Tada, Paris, & Irwin, 2000):

$$K(r) = K^{+}(r) + K^{-}(r), \tag{21}$$

with

$$K^{+}(r) = 2\Delta\tau\sqrt{\frac{r}{\pi}} \tag{22}$$

$$K^{-}(r) = 2\Delta\tau_{barr}\sqrt{\frac{r^2 - R^2}{r\pi}}, \tag{23}$$

$$\tag{24}$$

where $K^{+}(r)$ is the SIF due to a stress drop over the entire crack and $K^{-}(r)$ is the SIF due to an additional stress drop over the region $R \leq r \leq R_f$ where R_f is the final radius. We can write $\Delta\tau_{barr} = \alpha\Delta\tau$, where α is a factor representing the strength of the barrier causing rupture arrest; for numerical simulations used here (Appendix C), $(a-b)_{VS} = -(a-b)_{VW}$ and $\alpha = -2$. Plugging eq. 21 into 6 and solving for rupture velocity yields:

$$\frac{v_r(r)}{v_f} = 1 - \left(\sqrt{\tilde{r}} + \sqrt{\frac{\tilde{r}^2 - \tilde{R}^2}{\tilde{r}}}\right)^{-2}, \tag{25}$$

where $\tilde{r} = r/R_0$, $\tilde{R} = R/R_0$. I solve for rupture velocity as a function of time with the Matlab function `ode45`.

B Appendix: Pulses and source spectra for $\theta \neq 0$

Sato (1994) derived a surprisingly simple result to compute far-field displacement from circular sources propagating with variable rupture velocity. Let $T(r)$ be the time at which the rupture front reaches radius r, and define the quantities

$$T_a(r) = T(r) - r\sin\theta/c \tag{26}$$

$$T_b(r) = T(r) + r\sin\theta/c, \tag{27}$$

representing the range of arrival times for pulses emitted as the rupture grows from r to $r + dr$. The moment rate function is given by (Sato, 1994)

$$\dot{M}_c(t) = \frac{\pi\mu c a}{2\sin\theta}\left\{R_a(t)^2 - R_b(t)^2\right\}, \tag{28}$$

where R_a, R_b are the solution to $T_a(r) = t$ and $T_b(r) = t$ respectively and a a constant given by

$$a = \left(\frac{24}{7\pi}\right)\left(\frac{\Delta\tau}{\mu}\right). \tag{29}$$

Here I seek an analytical solution for small sources. Writing $R_a = R_0 + l_a$ and $R_b = R_0 + l_b$ and taking $l_{a,b} \ll R_0$, to first order we have: $R_a^2 - R_b^2 \approx 2R_0(l_a - l_b)$. At short times ($t \ll t_0$) the crack radius given by eq. 9 can be approximated as

$$r = R_0 + l_0 e^{t/t_0}, \tag{30}$$

where $l_0 = R_0\epsilon$ is defined as the radius in excess of R_0 at $t = 0$ (which can be arbitrarily small, and is used for mathematical convenience as explained in section 2). Inverting eq. 30 and combining with eq. 27 gives

$$l_a(t) = \min\left\{R - R_0, l_0 e^{t/t_0} e^{\Theta}\right\} \tag{31}$$

$$l_b(t) = \min\left\{R - R_0, l_0 e^{t/t_0} e^{-\Theta}\right\}, \tag{32}$$

with $\Theta = R\sin(\theta)/ct_0$. Using these expressions in eq. 28 gives the source time function. For convenience, I redefine t so that $t = 0$ corresponds to the peak of $\dot{M}_c(t)$ and obtain the following expression for the normalized source time function:

$$\dot{M}_c(t)/\dot{M}_c(0) = \begin{cases} e^{t/t_0} & t < 0 \\ \dfrac{e^{\Theta} - e^{-\Theta} e^{(t/t0)}}{e^{\Theta} - e^{-\Theta}} & 0 \le t < \Delta T \\ 0 & \Delta T \le t \end{cases} \tag{33}$$

with $\Delta T = T_b(R) - T_a(R)$. As before, I define the source duration as the time in which the displacement pulse exceeds a fraction ϕ of the maximum value, and obtain the following expression for the pulse duration:

$$T = t_0\left[\log\left(\frac{1}{\phi}\right) + \log\left(\frac{e^{\Theta} - 2\phi\sinh\Theta}{e^{-\Theta}}\right)\right]. \tag{34}$$

Taking the Fourier transform of eq. 33, and reintroducing the constants in eq. 11 yields the following source spectrum:

$$|\dot{M}_c(\omega)| = \frac{48\Delta\tau}{7}(R - R_0)R_0 R \,\mathrm{sinc}\left(\frac{\omega R\sin\theta}{c}\right)\frac{1}{\sqrt{\omega^2 t_0^2 + 1}}. \tag{35}$$

C Appendix: Dynamic rupture simulations

I run fully dynamic simulations using the boundary integral code *BICyclE* (Lapusta, Rice, Ben-Zion, & Zheng, 2000; Lapusta & Liu, 2009). The following equation of motion governs fault slip:

$$\tau_{el}(\mathbf{x}) - \tau_f(\mathbf{x}) = \frac{\mu}{2c_s}v(\mathbf{x}), \tag{36}$$

where μ is the shear modulus, τ_f the frictional resistance, τ_{el} the shear stress due to remote loading and elastodynamic stress interactions between elements, and the term on the right hand side represents radiation damping (Rice, 1993). Frictional resistance evolves according to rate-state friction (Marone, 1998):

$$\tau_f(v,\theta) = \sigma \left[f_0 + a \log \frac{v}{v^*} + b \log \frac{\theta v^*}{d_c} \right], \tag{37}$$

where, a, b and are constitutive parameters; $d_c = 10^{-4}$m is the state evolution distance; $\sigma =$ 50MPa is effective the normal stress; $v^* = 10^{-6}$m/s is a reference slip velocity; $f_0 = 0.6$ is the steady-state friction coefficient at $v = v^*$, and θ is a state-variable. I employ the ageing law (Ruina, 1983) for state evolution:

$$\frac{d\theta}{dt} = 1 - \frac{\theta v}{d_c}. \tag{38}$$

The model set up is similar to Chen and Lapusta (2009): I impose velocity weakening frictional parameters ($a - b = -0.005$, $b = 0.02$) within a circular asperity, and velocity strengthening parameters ($a - b = 0.005$) in a square region surrounding it. The fault is loaded by a velocity boundary condition $v = 10^{-9}$m/s. To minimize edge effects, the creeping region is at least 3 times larger than the asperity. Nucleation under ageing law with the parameters employed here takes the form of an expanding crack with the nucleation dimension given by:

$$R_\infty = \frac{\pi}{4} \frac{b}{(b-a)^2} \frac{\mu' d_c}{\sigma} \tag{39}$$

where μ' is the shear modulus for antiplane shear and the shear modulus divided by $1 - \nu$ ($\nu =$ Poisson's ratio) for plane strain deformation (with the parameters used here, $R_\infty = 38$m and 50m respectively).

Acknowledgments

I would like to thank Nadia Lapusta for sharing the *BICyclE* code and Valère Lambert for helping set up the simulations. I am grateful to Paul Segall, Rachel Abercrombie and Victor Tsai for stimulating discussions on these topics. This project was supported by NEHRP grant G19AP00020.

References

Abercrombie, R. E. (1995). Earthquake source scaling relationships from -1 to 5 M_l using seismograms recorded at 2.5-km depth. *Journal of Geophysical Research*, *100*(B12), 24015–24036.

Abercrombie, R. E. (2021, May). Resolution and uncertainties in estimates of earthquake stress drop and energy release. *Philosophical Transactions of the Royal Society A: Mathematical, Physical and Engineering Sciences*, *379*(2196), 20200131. Retrieved 2022-03-09, from https://royalsocietypublishing.org/doi/10.1098/rsta.2020.0131 (Publisher: Royal Society) doi: 10.1098/rsta.2020.0131

Aki, K. (1967). Scaling law of seismic spectrum. *Journal of Geophysical Research*, *72*(4), 1217–1231. (ISBN: 0148-0227) doi: 10.1029/JZ072i004p01217

Aki, K., & Richards, P. (1980). *Quantitative Seismology: Theory and Methods* (W. H. Freeman, Ed.). New York.

Atkinson, G. M., & Beresnev, I. (1997, January). Don't Call it Stress Drop. *Seismological Research Letters*, *68*(1), 3–4. Retrieved 2022-01-14, from https://pubs.geoscienceworld.org/srl/article/68/1/3-4/142155 doi: 10.1785/gssrl.68.1.3

Baltay, A., Ide, S., Prieto, G., & Beroza, G. (2011). Variability in earthquake stress drop and apparent stress. *Geophysical Research Letters*, *38*(6). Retrieved 2022-03-15, from https://onlinelibrary.wiley.com/doi/abs/10.1029/2011GL046698 (_eprint: https://onlinelibrary.wiley.com/doi/pdf/10.1029/2011GL046698) doi: 10.1029/2011GL046698

Bindi, D., Spallarossa, D., Picozzi, M., & Morasca, P. (2020, July). Reliability of Source Parameters for Small Events in Central Italy: Insights from Spectral Decomposition Analysis Applied to Both Synthetic and Real Data. *Bulletin of the Seismological Society of America*, *110*(6), 3139–3157. Retrieved 2022-03-09, from https://doi.org/10.1785/0120200126 doi: 10.1785/0120200126

Boatwright, J. (1980, February). A spectral theory for circular seismic sources; simple estimates of source dimension, dynamic stress drop, and radiated seismic energy. *Bulletin of the Seismological Society of America*, *70*(1), 1–27. Retrieved 2022-03-11, from https://doi.org/10.1785/BSSA0700010001 doi: 10.1785/BSSA0700010001

Bouchon, M., Karabulut, H., Aktar, M., Özalaybey, S., Schmittbuhl, J., & Bouin, M. P. (2011). Extended nucleation of the 1999 Mw 7.6 Izmit earthquake. *Science*, *331*(6019), 877–880. (ISBN: 1095-9203 (Electronic)\r0036-8075 (Linking)) doi: 10.1126/science.1197341

Brune, J. N. (1970). Tectonic stress and the spectra of seismic shear waves from earthquakes. *Journ. Geophys. Res.*, *75*(26).

Cattania, C., & Segall, P. (2019). Crack models of repeating earthquakes predict observed moment-recurrence scaling. *Journ. Geophys. Res.*, *124*(1), 476–503. Retrieved 2019-07-17, from https://agupubs.onlinelibrary.wiley.com/doi/abs/10.1029/2018JB016056 doi: 10.1029/2018JB016056

Chen, T., & Lapusta, N. (2009). Scaling of small repeating earthquakes explained by interaction of seismic and aseismic slip in a rate and state fault model. *Journal Geophys. Res.*, *114*, 1–12. doi: 10.1029/2008JB005749

Dieterich, J. H. (1992). Earthquake nucleation on faults with rate-and state-dependent strength. *Tectonophysics*, *211*(1-4), 115–134. (ISBN: 0040-1951) doi: 10.1016/0040-1951(92)90055-B

Dieterich, J. H., & Linker, M. F. (1992). Fault stability under conditions of variable normal stress. *Geophysical Research Letters*, *19*(16), 1691–1694. doi: 10.1029/92GL01821

Eshelby, J. (1957). Determination of the elastic field of an ellipsoidal inclusion, and related problems. *Proceedings of the Royal Society of London*. (arXiv: 1011.1669v3 ISBN: 00804630) doi: 10.1098/rspa.1957.0133

Freund, L. B. (1990). *Dynamic Fracture Mechanics*. Cambridge Monographs on Mechanics. Retrieved from https://www.cambridge.org/core/books/dynamic-fracture-mechanics/4518586440239B156F0C8AD8911E2 doi: 10.1017/CBO9780511546761

Harrington, R. M., & Brodsky, E. E. (2009). Source duration scales with magnitude differently for earthquakes on the San Andreas fault and on secondary faults in Parkfield, California. *Bulletin of the Seismological Society of America*, *99*(4), 2323–2334. (ISBN: 0037-1106) doi: 10.1785/0120080216

Ide, S., Beroza, G. C., Prejean, S. G., & Ellsworth, W. L. (2003). Apparent break in earthquake scaling due to path and site effects on deep borehole recordings. *Journal of Geophysical Research: Solid Earth*, *108*(B5). Retrieved from http://doi.wiley.com/10.1029/2001JB001617 (ISBN: 0148-0227) doi: 10.1029/2001JB001617

Imanishi, K., & Uchide, T. (2017). Non-self-similar source property for microforeshocks of the 2014 Mw 6.2 Northern Nagano, central Japan, earthquake. *Geophysical Research Letters*, *44*(11), 5401–5410. doi: 10.1002/2017GL073018

Kanamori, H., & Rivera, L. (2004, February). Static and Dynamic Scaling Relations for Earthquakes and Their Implications for Rupture Speed and Stress Drop. *Bulletin of the Seismological Society of America*, *94*(1), 314–319. Retrieved 2022-03-09, from https://doi.org/10.1785/0120030159 doi: 10.1785/0120030159

Kaneko, Y., & Shearer, P. M. (2014). Seismic source spectra and estimated stress drop derived from cohesive-zone models of circular subshear rupture. *Geophysical Journal International*, *197*(2), 1002–1015. doi: 10.1093/gji/ggu030

Kaneko, Y., & Shearer, P. M. (2015). Variability of seismic source spectra, estimated stress drop, and radiated energy, derived from cohesive-zone models of symmetrical and asymmetrical circular and elliptical ruptures. *Journal of Geophysical Research B: Solid Earth*, *120*(2), 1053–1079. (ISBN: 0148-0227) doi: 10.1002/2014JB011642

Kwiatek, G., & Ben-Zion, Y. (2013). Assessment of P and S wave energy radiated from very small shear-tensile seismic events in a deep South African mine. *Journal of Geophysical Research: Solid Earth*, *118*(7), 3630–3641. Retrieved 2022-03-15, from https://onlinelibrary.wiley.com/doi/abs/10.1002/jgrb.50274 (_eprint: https://onlinelibrary.wiley.com/doi/pdf/10.1002/jgrb.50274) doi: 10.1002/jgrb.50274

Lapusta, N., & Liu, Y. (2009). Three-dimensional boundary integral modeling of spontaneous earthquake sequences and aseismic slip. *Journal of Geophysical Research: Solid Earth*, *114*(B9). Retrieved 2020-05-12, from http://agupubs.onlinelibrary.wiley.com/doi/abs/10.1029/2008JB005934 (_eprint: https://onlinelibrary.wiley.com/doi/pdf/10.1029/2008JB005934) doi: 10.1029/2008JB005934

Lapusta, N., Rice, J. R., Ben-Zion, Y., & Zheng, G. (2000, October). Elastodynamic analysis for slow tectonic loading with spontaneous rupture episodes on faults with rate- and state-dependent friction. *Journal of Geophysical Research: Solid Earth*, *105*(B10). Retrieved 2019-02-15, from http://doi.wiley.com/10.1029/2000JB900250 (Publisher: John Wiley & Sons, Ltd) doi: 10.1029/2000JB900250

Leeman, J. R., Saffer, D. M., Scuderi, M. M., & Marone, C. (2016). Laboratory observations of slow earthquakes and the spectrum of tectonic fault slip modes. *Nat Commun*, *7*, 11104. Retrieved from http://www.ncbi.nlm.nih.gov/pubmed/27029996 (Publisher: Nature Publishing Group ISBN: 2041-1723 (Electronic)\r2041-1723 (Linking)) doi: 10.1038/ncomms11104

Lengliné, O., Lamourette, L., Vivin, L., Cuenot, N., & Schmittbuhl, J. (2014). Fluid-induced earthquakes with variable stress drop. *Journal of Geophysical Research: Solid Earth*, *119*(12), 8900–8913. Retrieved 2022-03-09, from https://onlinelibrary.wiley.com/doi/abs/10.1002/2014JB011282 (_eprint: https://onlinelibrary.wiley.com/doi/pdf/10.1002/2014JB011282) doi: 10.1002/2014JB011282

Lin, Y.-Y., & Lapusta, N. (2018). Microseismicity Simulated on Asperity-Like Fault Patches: On Scaling of Seismic Moment With Duration and Seismological Estimates of Stress Drops. *Geophysical Research Letters*, *45*(16), 8145–8155. Retrieved 2022-03-22, from https://onlinelibrary.wiley.com/doi/abs/10.1029/2018GL078650 (_eprint: https://onlinelibrary.wiley.com/doi/pdf/10.1029/2018GL078650) doi: 10.1029/2018GL078650

Lin, Y. Y., Ma, K. F., Kanamori, H., Alex Song, T. R., Lapusta, N., & Tsai, V. C. (2016). Evidence for non-self-similarity of microearthquakes recorded at a Taiwan borehole seismometer array. *Geophysical Journal International*, *206*(2), 757–773. doi: 10.1093/gji/ggw172

Madariaga, R. (1976). Dynamics of an expanding circular fault. *Bulletin of the Seismological Society of America*, *66*(3), 639–666. Retrieved from `http://bssa.geoscienceworld.org/content/66/3/639.abstract` (ISBN: 0037-1106)

Malagnini, L., Scognamiglio, L., Mercuri, A., Akinci, A., & Mayeda, K. (2008). Strong evidence for non-similar earthquake source scaling in central Italy. *Geophysical Research Letters*, *35*(17). Retrieved 2022-03-09, from `https://onlinelibrary.wiley.com/doi/abs/10.1029/2008GL034310` (_eprint: https://onlinelibrary.wiley.com/doi/pdf/10.1029/2008GL034310) doi: 10.1029/2008GL034310

Marone, C. (1998, May). Laboratory-derived friction laws and their application to seismic faulting. *Annual Review of Earth and Planetary Sciences*, *26*(1), 643–696. Retrieved from `http://www.annualreviews.org/doi/abs/10.1146/annurev.earth.26.1.643` doi: 10.1146/annurev.earth.26.1.643

Mayeda, K., Malagnini, L., & Walter, W. R. (2007). A new spectral ratio method using narrow band coda envelopes: Evidence for non-self-similarity in the Hector Mine sequence. *Geophysical Research Letters*, *34*(11). Retrieved 2022-03-09, from `https://onlinelibrary.wiley.com/doi/abs/10.1029/2007GL030041` (_eprint: https://onlinelibrary.wiley.com/doi/pdf/10.1029/2007GL030041) doi: 10.1029/2007GL030041

McLaskey, G. C. (2019, December). Earthquake initiation from laboratory observations and implications for foreshocks. *Journal of Geophysical Research: Solid Earth*, 2019JB018363. Retrieved 2019-12-20, from `https://onlinelibrary.wiley.com/doi/abs/10.1029/2019JB018363` doi: 10.1029/2019JB018363

Rice, J. R. (1993). Spatio-temporal complexity of slip on a fault. *Journal of Geophysical Research*, *98*(B6), 9885. (ISBN: 2156-2202) doi: 10.1029/93JB00191

Rubin, A. M., & Ampuero, J. (2005). Earthquake nucleation on (aging) rate and state faults. *Journal of Geophysical Research*, *110*(2), 1–24. doi: 10.1029/2005JB003686

Ruina, A. (1983). Slip instability and state variable friction law. *J. Geophys. Res.*, *88*, 10359–10370. Retrieved from http://onlinelibrary.wiley.com/doi/10.1029/JB088iB12p10359/abstract (ISBN: 0148-0227) doi: 10.1029/JB088iB12p10359

Sato, T. (1994, August). Seismic radiation from circular cracks growing at variable rupture velocity. *Bulletin of the Seismological Society of America*, *84*(4), 1199–1215. Retrieved 2022-01-14, from https://doi.org/10.1785/BSSA0840041199 doi: 10.1785/BSSA0840041199

Sato, T., & Hirasawa, T. (1973). Body wave spectra from propagating shear cracks. *Journal of Physics of the Earth*, *21*, 415–431. (ISBN: 0022-3743) doi: 10.4294/jpe1952.21.415

Selvadurai, P. A. (2019). Laboratory Insight Into Seismic Estimates of Energy Partitioning During Dynamic Rupture: An Observable Scaling Breakdown. *Journal of Geophysical Research: Solid Earth*, *124*(11), 11350–11379. Retrieved 2022-03-15, from https://onlinelibrary.wiley.com/doi/abs/10.1029/2018JB017194 (_eprint: https://onlinelibrary.wiley.com/doi/pdf/10.1029/2018JB017194) doi: 10.1029/2018JB017194

Shearer, P. M., Abercrombie, R. E., Trugman, D. T., & Wang, W. (2019). Comparing EGF Methods for Estimating Corner Frequency and Stress Drop From P Wave Spectra. *Journal of Geophysical Research: Solid Earth*, *124*(4), 3966–3986. Retrieved 2022-03-15, from https://onlinelibrary.wiley.com/doi/abs/10.1029/2018JB016957 (_eprint: https://onlinelibrary.wiley.com/doi/pdf/10.1029/2018JB016957) doi: 10.1029/2018JB016957

Tada, H., Paris, P. C., & Irwin, G. R. (2000). *The Stress Analysis of Cracks Handbook*. Hellertown PA: Del Research Corp. doi: 10.1115/1.801535

Trugman, D. T., & Shearer, P. M. (2017). Application of an improved spectral decomposition method to examine earthquake source scaling in Southern California. *Journal of Geophysical Research: Solid Earth*, *122*(4), 2890–2910. Retrieved 2022-03-09, from https://onlinelibrary.wiley.com/doi/abs/10.1002/2017JB013971 (_eprint: https://onlinelibrary.wiley.com/doi/pdf/10.1002/2017JB013971) doi: 10.1002/2017JB013971

Wang, H., Ren, Y., Wen, R., & Xu, P. (2019). Breakdown of Earthquake Self-Similar Scaling and Source Rupture Directivity in the 2016–2017 Central Italy Seismic Sequence. *Journal of Geophysical Research: Solid Earth*, *124*(4), 3898–3917. Retrieved 2022-03-09, from https://onlinelibrary.wiley.com/doi/abs/10.1029/2018JB016543 (_eprint: https://onlinelibrary.wiley.com/doi/pdf/10.1029/2018JB016543) doi: 10.1029/2018JB016543

Wang, Y., & Day, S. M. (2017). Seismic source spectral properties of crack-like and pulse-like modes of dynamic rupture. *Journal of Geophysical Research: Solid Earth*, *122*(8), 6657–6684. doi: 10.1002/2017JB014454

Yoshimitsu, N., Kawakata, H., & Takahashi, N. (2014). Magnitude -7 level earthquakes: A new lower limit of self-similarity in seismic scaling relationships. *Geophysical Research Letters*, *41*(13), 4495–4502. Retrieved 2022-03-15, from https://onlinelibrary.wiley.com/doi/abs/10.1002/2014GL060306 (_eprint: https://onlinelibrary.wiley.com/doi/pdf/10.1002/2014GL060306) doi: 10.1002/2014GL060306

Zollo, A., Orefice, A., & Convertito, V. (2014). Source parameter scaling and radiation efficiency of microearthquakes along the Irpinia fault zone in southern Apennines, Italy. *Journal of Geophysical Research: Solid Earth*, *119*(4), 3256–3275. Retrieved 2022-03-09, from https://onlinelibrary.wiley.com/doi/abs/10.1002/2013JB010116 (_eprint: https://onlinelibrary.wiley.com/doi/pdf/10.1002/2013JB010116) doi: 10.1002/2013JB010116